Journal of Power Sources 196 (2011) 10465–10471

Contents lists available at ScienceDirect

Journal of Power Sources

journal homepage: www.elsevier.com/locate/jpowsour

A high-performance three-dimensional micro supercapacitor based on self-supporting composite materials☆

Caiwei Shen[a,b], Xiaohong Wang[a,b,*], Wenfeng Zhang[a,c], Feiyu Kang[a,c]

[a] Tsinghua National Laboratory for Information Science and Technology, PR China
[b] Institute of Microelectronics, Tsinghua University, Beijing 100084, PR China
[c] Department of Materials Science and Engineering, Tsinghua University, Beijing 100084, PR China

ARTICLE INFO

Article history:
Received 26 May 2011
Accepted 2 August 2011
Available online 9 August 2011

Keywords:
Micro supercapacitor
Three-dimensional electrodes
Self-supporting composite

ABSTRACT

This paper introduces a silicon three-dimensional (3D) micro supercapacitor, featured by using self-supporting nano porous composite materials and interdigital electrodes with high-aspect-ratio. A way to prepare self-supporting materials has been developed, and composites that contain an activated carbon as the active component have been studied and designed to meet the requirements for adequate specific capacitance, good conductivity and strong structure. By combining the designed composite with microfabrication techniques, a micro supercapacitor with high-aspect-ratio interdigital electrodes has been achieved. Electrochemical characterization results of the prototype with $NaNO_3$ electrolyte demonstrate that the 3D supercapacitor exhibits an outstanding overall performance. A large capacitance of 90.7 mF cm^{-2} and a fast power of 51.5 mW cm^{-2} are calculated. Robust stability and high charge/discharge efficiency are also observed. Moreover, this study provides a scalable device built by compatible fabrication method, which is applicable to the integration of high-performance supercapacitors on chip.

1. Introduction

Today's rapid growth of portable electronic equipment, wireless sensor networks and other micro systems is driving an increasing demand for better energy storage and power supply under various conditions. At the same time, the desire to further miniaturize existing on-chip systems makes it attractive to develop power devices integrated with other elements. The use and combination of electrochemical rechargeable devices such as batteries and supercapacitors are possible solutions. In fact, even when electricity can be generated by fuel cell [1] or energy harvesting method [2,3], these rechargeable components are indispensable for consistent power supply. Li-ion batteries have attracted a lot of attention because of their high energy density and flexibility, and their micro structures have been closely investigated because of the merit that their diffusion lengths are decreased and the fraction of electroactive materials is increased [4]. However, micro batteries still suffer from fundamental problems caused by the electrochemical reactions they are based on: relatively poor charge/discharge rates and limited cycle life (hundreds to thousands of cycles) are inevitable in those redox reactions [4,5].

Electrochemical capacitors (ECs), also called supercapacitors, store energy using either electrochemical double layer (EDL) effect or fast surface redox reactions (pseudo capacitance) happen on the interface of electrodes and electrolytes [6,7]. These mechanisms ensure fast charge and discharge rates (compared with rechargeable batteries) and long cycle life (millions of cycles) of ECs, and the development of advanced nanostructured materials makes ECs keep a reasonable energy density (sometimes even close to that of batteries) [7]. Due to these advantages, ECs can serve as a major complement to batteries, or even substitute for them, in energy storage and harvesting applications, and the recent interest in extending their application to micro power systems is not unexpected [8–17].

Notable work has been done on micro supercapacitors, the main goal of which has been to improve their performance in a limited area by using high-capacity active materials and 3D structures. In particular, micro supercapacitors have not just been scaled down from large-sized ones. A volumetric capacity exceeding that of macroscale supercapacitors has been observed in micrometre-scale carbide derived carbons [13], and an ultrahigh volumetric power has also been presented in an on-chip device with a micro structure [16]. Therefore, good micrometre-sized structures are especially important to improve the performance of micro supercapacitors.

☆ This manuscript is based on the IEEE International Conference on Micro Electro Mechanical Systems (MEMS 2011) Technical Digest contribution, "A Novel Three-Dimensional Micro Supercapacitor Using Self-support Nano Composite Materials".

* Corresponding author at: Institute of Microelectronics, Tsinghua University, Beijing 100084, PR China. Tel.: +86 10 62789151x317; fax: +86 10 62771130.
E-mail address: wxh-ime@tsinghua.edu.cn (X. Wang).

0378-7753/$ – see front matter.
doi:10.1016/j.jpowsour.2011.08.007

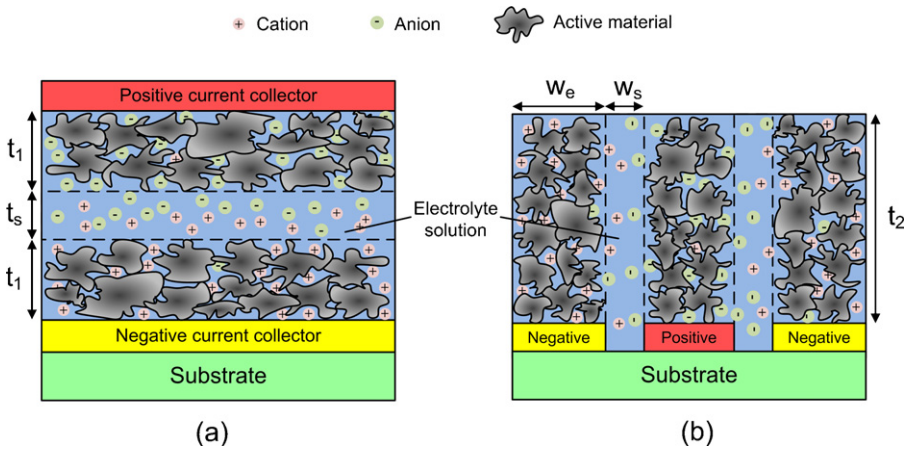

Fig. 1. (a) Diagram of a supercapacitor with a sandwich structure. The thickness of the active material in each electrode is t_1 and the thickness of space between electrodes is t_s. (b) Diagram of a supercapacitor with an interdigital structure. Electrodes with a thickness of t_2 and a width of w_e are separated by a width of w_s.

Micro supercapacitors can be classified by structure into sandwich [8], roll-like [9] and interdigital [10–15]. The interdigital structure has advantages over the others, including its possible extension from three dimensions, which allows more materials to be loaded per unit area with thicker electrodes, and easy adjustment of the patterns, which can decrease the internal impedance by minimizing the distance between two electrodes. Sun et al. [10,11] fabricated micro supercapacitors with polymerized polypyrrole (PPy) films coated on interdigital structures. The performance of their devices is limited by the thin active layer of electrodes, as well as the wide spaces between electrodes that are hard to be narrowed by using electroplating to grow the active material. Pech et al. [12,13] built interdigital electrodes using carbon materials. However, the printing [12] and electrophoretic deposition [13] methods cannot be used to fabricate thick electrodes with minimal gaps in between, and the materials they used are not likely to support by themselves. Another strategy to obtain high-aspect-ratio electrodes is to synthesize the material directly on the substrate, such as by using chemical vapor deposition (CVD). But the known examples suffer from the low volume density of the material, such as vertically grown carbon nanotubes [14,15], or a serious drop in capacity when the electrodes grow thicker, such as carbide derived carbons [16]. Besides, direct growth of the materials on substrates often requires very high temperatures, which limit their potential to be integrated with other micro devices.

In this study, a high-aspect-ratio interdigital structure for three-dimensional micro supercapacitor is achieved by combining deep etching techniques with self-supporting active materials. In particular, the concept of using flexible composites instead of pure active materials for self-supporting electrodes is demonstrated. The prototype using activated carbon as active material has been characterized, and the performance is exceedingly high, as expected. The scalable device built by compatible fabrication method is also a step towards integration.

2. Strategies and materials

2.1. Principles and strategies

To store electrical energy in the two electrodes of a supercapacitor, cations and anions in the ion-conducting electrolyte solution will separate, migrate and accumulate on the surface of the active materials, where EDLs are formed or fast surface redox reactions happen. To release the power, ions will go in the opposite direction. Those processes can be briefly illustrated in Fig. 1a. The capacity of a supercapacitor depends heavily on the total surface area of its electrodes, because with a larger surface area, both EDL and surface redox reaction can store more charges. The charge/discharge rates are closely related to the migration distance of ions in the electrolyte, and the impedance of a supercapacitor can be lowered by shortening this path [6].

As for supercapacitors that are limited in a fixed volume, the structure of their electrodes can be very important. Two supercapacitors, which have different structures but the same volume, are illustrated in Fig. 1. If a certain electrode material is used in a sandwich structure shown in Fig. 1a, the capacity of the supercapacitor is proportional to the ratio of volume that contains active material, i.e. $2t_1/(2t_1 + t_s)$. And the average migration distance of ions in charge/discharge processes are related to t_1 and t_s, which means both the thickness of electrodes and that of the space between electrodes affect the charge/discharge rates. Similarly, in an interdigital structure shown in Fig. 1b, whose electrodes are separated on the same plane, the capacity is proportional to the ratio w_e/w_s. And the average migration distance of ions is related to w_e and w_s.

The area of substrate, however, is always limited in the case of micro supercapacitors. In a fixed substrate area, the only way to improve capacity in a sandwich supercapacitor is to increase t_1, but that will make the migration distance of ions larger, which means slower charge/discharge rates of the supercapacitor. While in an interdigital supercapacitor, the capacity can be improved by increasing the thickness of all electrodes, t_2, and the migration distance of ions is not directly increased. Moreover, w_e and w_s can be easily adjusted in interdigital electrodes so that the average migration distance of ions can be controlled. In a word, designing the interdigital structure well can exploit the advantages of three-dimensional micro supercapacitors to the full.

The above analyses lead to our basic principles to design the micro supercapacitor: The porous electrodes need to grow thick and still maintain their porosity, so that the total surface area can be large and offer a large capacity; and the electrodes need to be narrow and very close to each other, so that the migration distance of ions can be short and result in a fast charge/discharge rate.

The fabrication strategies were designed accordingly, which are illustrated in Fig. 2. In the 1st step, high-aspect-ratio interdigital channels are formed on substrate, with a wall between fingers. An insulation layer and then a metal layer are deposited in step 2, where the metal layer serves as current collector and the insulation layer prevents current leakage through substrate. In step 3, a self-supporting electrode material is filled into the channels to stack to a 3D structure, where the wall between channels ensures a perfect separation of two electrodes. Finally, the wall is etched and the space is left for electrolyte in step 4. The key point of the above

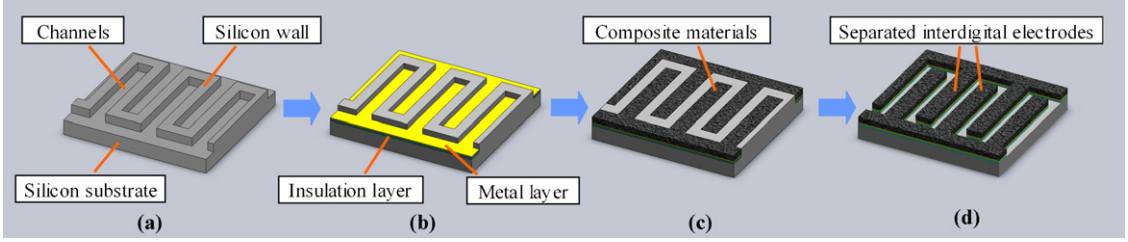

Fig. 2. Steps to form 3D electrodes: (a) etch the substrate to form deep channels; (b) deposit an insulation layer and then a metal layer as the current collector, the unnecessary layers on the top of the wall are removed by lithography and etching; (c) fill the channels with electrode materials; (d) etch the wall between two electrodes.

strategies is that, assisted by a silicon wall, the self-supporting material can grow thick and be perfectly separated.

2.2. Material design and experiments

The self-supporting electrode material mentioned above should not only be able to accomplish the fabrication strategies, but also have fine qualities including excellent electrochemical capacitance and sufficient conductivity. We find that composite material that combines electrochemical active materials and polymer binders can meet those requirements well. In fact, using composites rather than pure active materials can be more flexible and alterable, because the selection of active components of the composite can be various. In this paper, activated carbons are first considered as the active component because of their large specific surface areas caused by nano porous structures, which in most cases lead to large specific EDL capacitance [18–20]. Therefore, the electrode material used in this paper has been designed and prepared as follows: powder of activated carbon with large specific surface area (1000 $m^2\,g^{-1}$, BET) and high volume density (0.7 $g\,cm^{-3}$) was chosen as the active component. Graphite powder was added to increase the conductivity. A polymer binder, PVDF, was dissolved in N-methyl-2-pyrrolidone (NMP), and then mixed with the above components to form a suspension. The suspension was injected into the micro channels and became solid, or self-supporting, after drying. In this way, active materials that were not able to stand or gather tightly by themselves were bound together by polymers.

Enough amount of polymer binder in the composite is important, because it ensures the self-support and reliability of the material. However, it should be noticed that by adding polymer binders, some of the micro pores of the carbons are blocked by polymer molecules, and the surface area decreases, EDL capacitance that is proportional to surface area drops as a result [21–23]. So polymer binders should not occupy a large proportion of the composite. In order to examine this effect quantitatively, comparative experiments have been carried out on pure activated carbon (denoted as M1) and three types of composite (M2–4). To verify the feasibility of self-supporting composite materials, more polymer than was needed was added. Among the composites, M2 consisted of 90 wt% activated carbon (AC) and 10 wt% PVDF; M3 was made up of 80 wt% AC, 10 wt% PVDF and 10 wt% carbon graphite (CG, powders with diameters around 1 μm); and M4 was composed of 80 wt% AC, 10 wt% PVDF and 10 wt% multi-wall carbon nanotubes (CNT, 1–2 μm long, 20 nm in diameter). All composites were prepared in the same way: PVDF was dissolved in NMP, and then mixed with the other components. The mixed suspensions were dried until NMP evaporated completely. Their surface area analyses were conducted by ASAP 2010 and the results are recorded in Table 1. The area denoted S_{AC} is BET surface area divided by the weight percentage of AC, which can be used to estimate the variance of pore structures of AC in different composites.

The surface area tests show that all materials have nano porous structures. Most of their surface areas are caused by micro pores with diameters less than 2 nm, and the median pore diameters are less than 1 nm. Comparing the results of composite materials (M2–4) with that of pure AC (M1), it can be seen that more than a half of the surface of AC has been reduced when polymers was added. This is probably because the polymer molecules block the porous structure of the activated carbon. In addition, the use of solvent can make the polymer form a coating layer on the carbon particles, which lead to a further reduction of micro pores [21]. Another phenomenon was that more surface area was lost by adding conductive agents, especially when using CNT, which may indicate that conductive agents help polymers block more pores. More experiments need to be conducted to understand the mechanism behind this effect. As the highly porous structure of the activated carbon is eventually maintained to a certain extent, we take an overall consideration of adequate surface area, good conductivity and strong structure of the composite, and design the percentages of each component to be: 80 wt% for activated carbon, 10 wt% for graphite and 10 wt% for PVDF.

3. Fabrication

The practical fabrication process followed the designed steps as shown in Fig. 2. To form interdigital channels, an aluminium layer was sputtered on the silicon wafer as a masking layer for the following inductively coupled plasma (ICP). Then lithography and ICP were applied to etch the channels, each finger of the channels was etched to be 105 μm wide and 90 μm deep, and the silicon wall between fingers was 15 μm wide. A 300 nm thick SiO_2 as insulation layer was deposited by plasma enhanced chemical vapor deposition

Table 1
Surface areas and median pore diameters of different materials.

No.	Components	S_{BET} ($m^2\,g^{-1}$)	S_{micro} ($m^2\,g^{-1}$)	S_{AC} ($m^2\,g^{-1}$)	d_m (nm)
M1	AC	994.9	819.6	994.9	0.580
M2	AC + PVDF	370.2	276.1	411.3	0.679
M3	AC + CG + PVDF	269.9	269.7	337.4	0.647
M4	AC + CNT + PVDF	182.2	129.8	227.8	0.705

S_{BET}, BET surface area of the material.
S_{micro}, surface area produced by micro pores (diameters less than 2 nm).
S_{AC}, BET surface area divided by the weight percentage of AC.
d_m, median pore diameter.

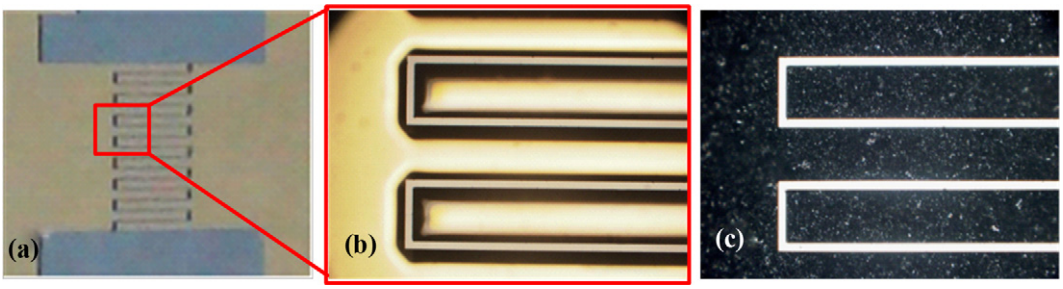

Fig. 3. Photographs of a cell in different procedures: (a) top view of the cell with interdigital channels separated by a silicon wall, a gold layer at the bottom of the channels serves as the current collector; (b) micrograph of a certain part of the cell without any electrode materials; (c) micrograph of the cell when the channels are filled with electrode materials.

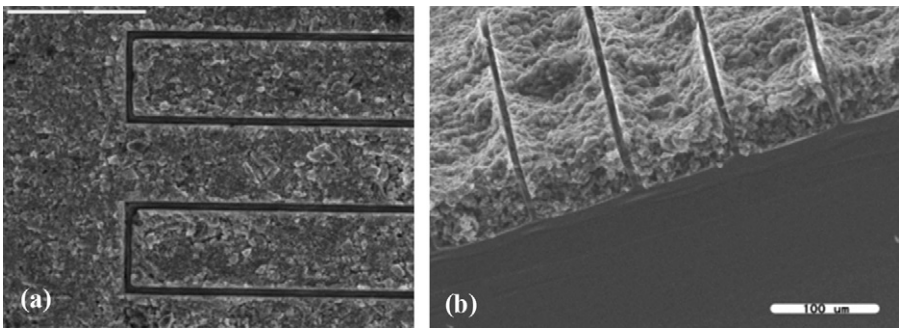

Fig. 4. SEM graphs of the cell after the silicon wall between electrodes are etched: (a) the top view of the interdigital electrodes; (b) the cross section view, and the white bar in this SEM graph is 100 μm long.

(PECVD), and then a 10 nm/100 nm Ti/Au as current collector layer by evaporation deposition. The unwanted layers on the top of the silicon wall, which would prevent ICP etching in the last step, were partially etched. Fig. 3a and b shows the photos of a cell that has interdigital channels with current collector layers at the bottom. Assisted by a microscope, the suspension of the composite material described in Section 2.2 of this paper was injected into the channels and then dried under 80–120 °C. As the material shrinks after the solvent evaporates, the inject-dry process has been repeated several times to fill as much material as possible into the channels. The tightly stacked material and full channels are shown in Fig. 3c.

A second ICP was applied to etch the silicon wall between electrodes, after which, no harm to the electrodes and current collector was observed. A top view of the separated electrodes was taken by SEM, shown in Fig. 4a and b, shows the cross section view. Because of the fluidity of the suspension and the heterogeneous heat distribution during the drying process, a rough surface on the top of the electrodes was shaped. The thickness of the final electrodes varies from 50 μm to 70 μm, which is thinner than but relative to the initial depth of the channels. High temperature treatment has been avoided here, and all dimensions are scalable by adjusting patterns and etching depth.

Fig. 5 shows the photo of a cell before package, where the black part in the middle of the cell is the interdigital electrodes region, with an effective area of 2 mm × 3 mm = 0.06 cm^2. The prototype was then assembled by a PDMS cap, with electrolyte (1 M $NaNO_3$) injected into the effective area.

4. Results and discussion

4.1. Specific capacitance and power

The electrochemical properties of the prototype were characterized by CHI 860D electrochemical workstation. Fig. 6a shows cyclic voltammetry (CV) curves of the prototype and the cell with bare gold, both at a scanning rate of 50 mV s^{-1}. Currents of the prototype are three orders larger, and the nearly rectangular shape represents a very good capacitive property. The capacitance of the device can be estimated by formula (1):

$$C = \frac{I}{dV/dt} \quad (1)$$

where I is the current on the CV curve and dV/dt is the scanning rate. At 0 V, the capacitance is calculated to be 5.44 mF. As the effective area (the area with active material) of the prototype is 0.06 cm^2, a specific capacitance of 90.7 mF cm^{-2} is deduced.

To take a larger-sized electrode as a reference, the specific capacitance of the material was measured in a three-electrode system. The suspension of the composite material was coated onto nickel

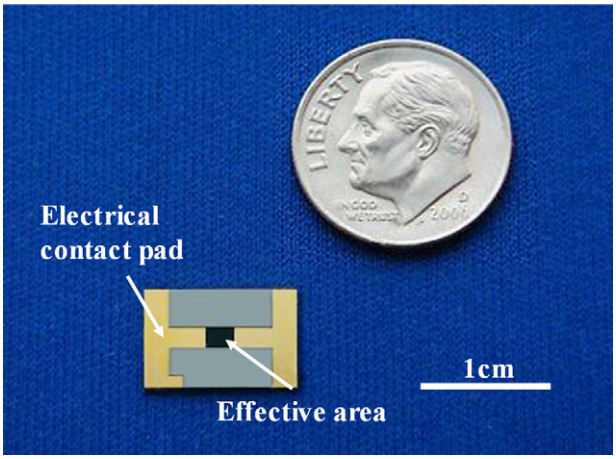

Fig. 5. Photo of a cell before package, the black part in the middle of the cell is the effective area with interdigital electrodes.

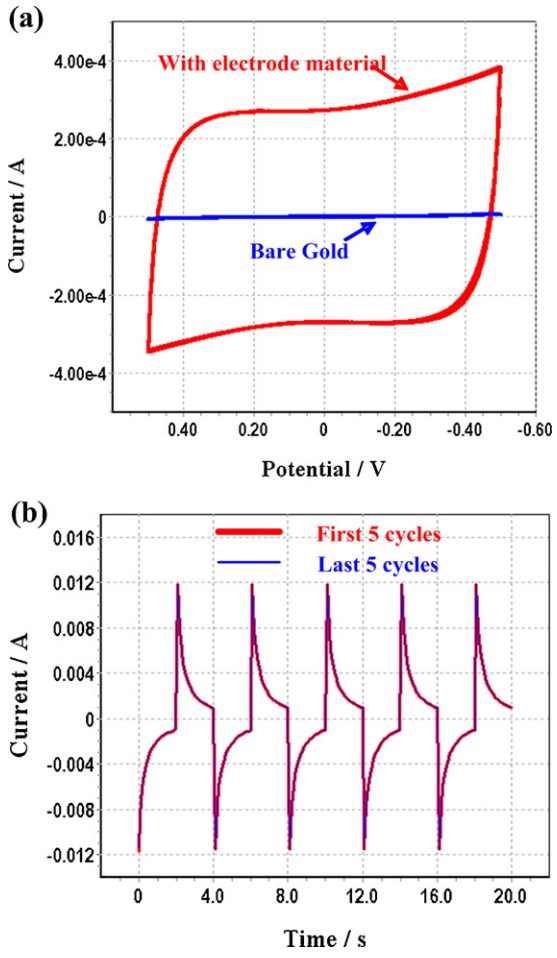

Fig. 6. (a) Cyclic voltammetry curves of the prototype (red line) and the cell with bare gold (blue line), both at the scanning rate of 50 mV s^{-1}. (b) Charge/discharge curves from 0 to 1 V. The red curve is the initial 5 periods, the blue one is another 5 periods after 100 cycles. (For interpretation of the references to color in this figure legend, the reader is referred to the web version of the article.)

foam substrate. The nickel foam was then pressed and dried to be an active electrode. The size of the electrode was about 150 μm thick and 0.5 cm^2 large. Cyclic voltammetry tests were conducted, but the CV curves of the electrode showed nearly rectangular shapes only when the scanning rate was below 10 mV s^{-1}. A capacitance of 96 F g^{-1} was measured at a scanning rate of 3 mV s^{-1} in 1 M $NaNO_3$ electrolyte.

The volume density of the composite was also estimated by drying the suspension in a regular shaped mold, and the value is 0.81 g cm^{-3}. Then a theoretical capacitance of the micro prototype can be expected by the following calculation: Assuming that the average thickness of the electrodes is 50 μm, then the mass of electrode material loaded in 1 cm^2 would be 50×10^{-4} $cm^3 \times 0.81$ g $cm^{-3} = 4.05$ mg (the space between electrodes has been ignored). As the material is allocated equally in two electrodes, each contains 4.05/2 = 2.025 mg and offers a capacitance of 2.025 mg × 96 F g^{-1} = 194.4 mF. Two electrodes are in series, resulting in a total capacitance of 194.4 mF/2 = 97.2 mF. In a word, a micro supercapacitor with 50 μm thick electrodes is expected to offer a specific capacitance of nearly 97.2 mF cm^{-2}, by using the composite electrode material in this paper. This calculation matches measured results of the prototype well, however, the capacitances of the prototype and the larger electrode are calculated based on measurements at different scanning rates. As is well known, keeping CV curves rectangular at higher scanning rates means lower resistive contributions in EDL capacitors [6,13]. Thus,

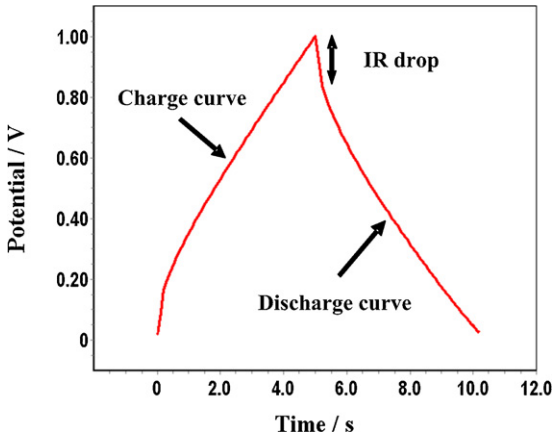

Fig. 7. A galvanostatic test of the prototype, at a charge/discharge current of 1 mA (16.67 mA cm^{-2}).

the micro supercapacitor here shows a better capacitive behavior than larger-sized electrodes.

In a chronoamperometry test, the device was charged and discharged between 0 and 1 V for more than 100 cycles. The coincidence of the first 5 periods and the last 5 periods of the curve in Fig. 6b shows a very good stability. Besides, the average power can be deduced from this curve, using Eq. (2):

$$\bar{P} = \frac{1}{T}\int_{t}^{t+T} VIdt \tag{2}$$

where T is the charge or discharge time, V is the voltage, and I is the current recorded on the curve. An average power of 3.09 mW (51.5 mW cm^{-2}) is calculated in a half cycle of the test. One way to evaluate the meaning of the specific power measured here would be to divide the power by the mass of the material loaded on the chip, that is, 51.5 mW/4.05 mg = 12.7 W g^{-1} (12.7 kW kg^{-1}). This value is larger than most large-scale supercapacitors using activated carbon as electrodes [4,19,20], the result is mainly attributed to the short distance between two electrodes in this device. In fact, the diffusion path of the ions in electrolyte, which affects the charge and discharge rates directly, can be shortened by narrowing the gap between electrodes as well as the width of each finger in the interdigital structure. Therefore, the specific power of the interdigital micro supercapacitor can be easily adjusted by using different patterns in lithography.

4.2. The galvanostatic experiment

A galvanostatic test was also conducted with a charge/discharge current of 1 mA (16.67 mA cm^{-2}), shown in Fig. 7. The charging half and discharging half of the curve are both straight lines when excluding the IR drops. A discharge capacitance can also be deduced from the curve after the IR drop, according to Eq. (3):

$$C = \frac{I \times \Delta t}{\Delta V \times A} \tag{3}$$

where I is the current, Δt is the time interval for the change in voltage range ΔV and A is the effective area of the prototype. The result is 98.9 mF cm^{-2} in this calculation, which is close to the value obtained from CV test. The charge/discharge efficiency here is 100%, for the charge time is equal to discharge time. This illustrates the complete reversibility of charge storage based on EDL capacitance.

Table 2
Summary of on-chip micro supercapacitors in the literature.

Structure	Electrode material	Electrolyte	Specific capacitance ($mF\,cm^{-2}$)	Specific power ($mW\,cm^{-2}$)	Reference
Sandwich	Carbon black	1.5 M H_2SO_4	~0.816[a]	NA^{-1}	In et al. [8]
Roll-like	RuO_2	0.5 M H_2SO_4	2.2	NA^{-1}	Ji et al. [9]
Interdigital	PPy films	$LiClO_4/H_2O$/PVA	30	2 (max)	Sun et al. [10]
	PPy films	0.5 M NaCl	56	0.56	Sun et al. [11]
	Activated carbon	1 M Et_4NBF_4 propylene carbonate	2.1	44.9 (max)	Pech et al. [12]
	Onion-like carbon	1 M Et_4NBF_4 propylene carbonate	0.9	~700 (max)[b]	Pech et al. [13]
	Carbon nanotube forests	[BMIM][BF_4]	0.428	0.28 (average)	Jiang et al. [14]
	Nickel electroplated carbon nanotube	0.1 M NaOH	26.7	NA^{-1}	Jiang et al. [15]
	Activated carbon	1 M $NaNO_3$	90.7	51.5 (average)	This work

[a] Capacitance of the device divided by the effective area provided in the paper.
[b] Estimated according to the dimensions of the device and the volumetric power density provided.

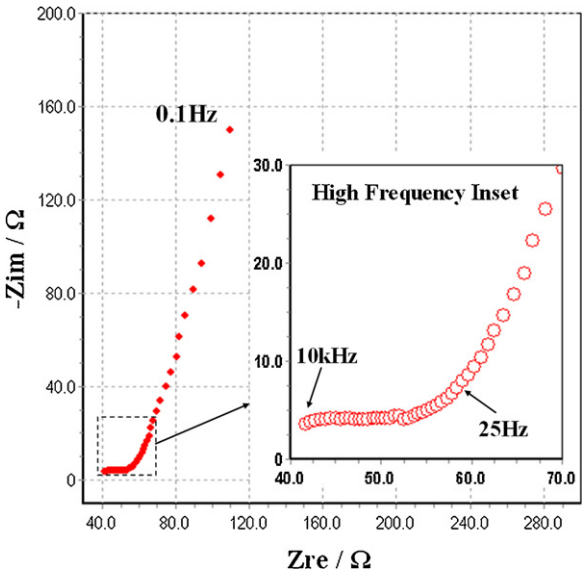

Fig. 8. The Nyquist plot of the micro supercapacitor. The impedances are measured at a bias of 0 V, under frequencies from 0.1 Hz to 10 kHz.

4.3. The impedance spectrum

Electrochemical impedance spectrum of the prototype was measured and the Nyquist plot is shown in Fig. 8. The quick increase of the imaginary part from 25 Hz down to 0.1 Hz indicates a capacitive behavior of the device. However, a leak resistance can be seen from the slope with an angle lower than 90° [24], and a series resistance of nearly 40 Ω can be deduced at the point where the curve interact with lateral axis. The series resistance is probably attributed to the contact resistance of the device with external circuit, by reducing which, the prototype can perform even better.

4.4. Comparisons of the results

Table 2 compares the specific capacitance and power of on-chip micro supercapacitors published in the literature. The device presented in this paper shows highly competitive energy storage and power delivery properties. Without using the material of the largest volumetric capacitance, the measured capacitance per unit area of this micro supercapacitor is obviously greater than other reported ones. Essential reasons are the combined factors of a heavy load of electrode material per unit area and the relatively large specific capacitance of the material. Moreover, among devices with interdigital electrodes, our device presents a fairly high specific power density. Regardless of the nano porous structures of the material, it achieves the narrowest micro gap between electrodes. The narrowed gap is beneficial for the improvement of both the capacitance per unit area and the power delivery of the device, because it increases the proportion of area that contains active material and reduces the migration distance of ions in the electrolyte, as illustrated in Section 2.1. Other methods of minimizing this gap by simply gathering materials onto current collectors [10–13] or vertically growing electrodes on substrates [13–16] are less satisfactory, because in those ways, the separation of the two electrodes cannot be ensured when the materials grow thicker.

5. Conclusions

A novel silicon three-dimensional micro supercapacitor based on self-supporting nano porous composite materials has been designed, fabricated and characterized. Deep etching processes are applied to achieve a high-aspect-ratio interdigital structure, and a way to prepare self-supporting composites with various active materials is introduced for application to micro supercapacitors. A large specific capacitance of 90.7 $mF\,cm^{-2}$ has been deduced in this paper, which is attributed to the combination of the three-dimensional structure and the nano porous material. An average power of 51.5 $mW\,cm^{-2}$, or about 12.7 $kW\,kg^{-1}$, has been calculated. The relatively fast charge/discharge rate is explained by the short electrolyte path length of the micro interdigital structure. The results of this work have been compared with those from other on-chip supercapacitors, and an outstanding overall performance is demonstrated. We believe this scalable micro supercapacitor built by compatible fabrication method will be applicable to different micro systems such as micro power suppliers or energy storage devices.

Acknowledgements

This work is supported by the National Natural Science Foundation (No. 60936003), 973 program (No. 2009CB320304), and 863 program (No. 2009AA04Z 319) of China.

References

[1] M. Winter, R.J. Brodd, Chem. Rev. 104 (2004) 4245–4269.
[2] S.P. Beeby, M.J. Tudor, N.M. White, Meas. Sci. Technol. 17 (2006) R175–R195.
[3] K.A. Cook-Chennault, N. Thambi, A.M. Sastry, Smart Mater. Struct. 17 (2008).
[4] J.W. Long, B. Dunn, D.R. Rolison, H.S. White, Chem. Rev. 104 (2004) 4463–4492.
[5] M. Armand, J.M. Tarascon, Nature 451 (2008) 652–657.
[6] B.E. Conway, Electrochemical Supercapacitors: Scientific Fundamentals and Technological Applications, Kluwer, New York, 1999.
[7] P. Simon, Y. Gogotsi, Nat. Mater. 7 (2008) 845–854.
[8] H.J. In, S. Kumar, Y. Shao-Horn, G. Barbastathis, Appl. Phys. Lett. 88 (2006) 083104.
[9] H.X. Ji, Y.F. Mei, O.G. Schmidt, Chem. Commun. 46 (2010) 3881–3883.
[10] W. Sun, X.Y. Chen, Microelectron. Eng. 86 (2009) 1307–1310.
[11] W. Sun, R.L. Zheng, X.Y. Chen, J. Power Sources 195 (2010) 7120–7125.
[12] D. Pech, M. Brunet, P.L. Taberna, P. Simon, N. Fabre, F. Mesnilgrente, V. Conedera, H. Durou, J. Power Sources 195 (2010) 1266–1269.

[13] D. Pech, M. Brunet, H. Durou, P.H. Huang, V. Mochalin, Y. Gogotsi, P.L. Taberna, P. Simon, Nat. Nanotechnol. 5 (2010) 651–654.
[14] Y.Q. Jiang, Q. Zhou, L. Lin, IEEE 22nd International Conference on Micro Electro Mechanical Systems. MEMS 2009, 2009, pp. 587–590.
[15] Y.Q. Jiang, P.B. Wang, J. Zhang, W. Li, L.W. Lin, IEEE 23rd International Conference on Micro Electro Mechanical Systems. MEMS 2010, 2010, pp. 1171–1174.
[16] J. Chmiola, C. Largeot, P.L. Taberna, P. Simon, Y. Gogotsi, Science 328 (2010) 480–483.
[17] M. Kaempgen, C.K. Chan, J. Ma, Y. Cui, G. Gruner, Nano Lett. 9 (2009) 1872–1876.
[18] B.E. Conway, V. Birss, J. Wojtowicz, J. Power Sources 66 (1997) 1–14.
[19] E. Frackowiak, F. Beguin, Carbon 39 (2001) 937–950.
[20] A.G. Pandolfo, A.F. Hollenkamp, J. Power Sources 157 (2006) 11–27.
[21] V. Ruiz, C. Blanco, M. Granda, R. Menendez, R. Santamaria, J. Appl. Electrochem. 37 (2007) 717–721.
[22] C.C. Hu, C.C. Wang, J. Power Sources 125 (2004) 299–308.
[23] A.B. Fuertes, F. Pico, J.M. Rojo, J. Power Sources 133 (2004) 329–336.
[24] B.E. Conway, W.G. Pell, T.C. Liu, J. Power Sources 65 (1997) 53–59.